# Single cell analysis of the aging hypothalamus

Kaitlyn H. Hajdarovic[1], Doudou Yu[2], Lexi-Amber Hassell[3], Shane Evans[4], Nicola Neretti[3,5], Ashley E. Webb[3,5,6,7]*

[1]Graduate program in Neuroscience, Brown University, Providence, RI, 02912, USA.
[2]Graduate program in Molecular Biology, Cell Biology, and Biochemistry, Brown University, Providence, RI 02912, USA.
[3]Department of Molecular Biology, Cell Biology, and Biochemistry, Brown University, Providence, RI 02912, USA.
[4]Graduate program in Computational Biology, Brown University, Providence, RI, 02912, USA.
[5]Center on the Biology of Aging, Brown University, Providence, RI 02912, USA.
[6]Carney Institute for Brain Science, Brown University, Providence, RI 02912, USA.
[7]Center for Translational Neuroscience, Brown University, Providence, RI 02912, USA.

*Correspondence to:
Dr. Ashley Webb
Ashley_Webb@brown.edu
401-863-6840

Key words: Aging, Hypothalamus, Single cell RNA-seq, Brain

## ABSTRACT

Alterations in metabolism, sleep patterns, body composition, and hormone status are all key features of aging. The hypothalamus is a well-conserved brain region that controls these homeostatic and survival-related behaviors. Despite the importance of this brain region in healthy aging, little is known about the intrinsic features of hypothalamic aging. Here, we utilize single nuclei RNA-sequencing to assess the transcriptomes of 22,718 hypothalamic nuclei from young and aged female mice. We identify cell type-specific signatures of aging in neurons, astrocytes, and microglia, as well as among the diverse collection of neuronal subtypes in this region. We uncover key changes in cell types critical for metabolic regulation and body composition, as well as in an area of the hypothalamus linked to cognition. In addition, our analysis reveals female-specific changes in sex chromosome regulation in the aging brain. This study identifies critical cell-specific features of the aging hypothalamus in mammals.

## INTRODUCTION

While human lifespan has increased dramatically in recent years, improvements in healthspan, the period of life in which a person is disease-free, have been more modest[1]. Susceptibility to a host of diseases increases with aging, including diabetes, stroke[2], cancer[3], and neurodegenerative diseases[4]. Aging is accompanied by changes in body composition, including decreased lean muscle mass, loss of bone density, and increased abdominal fat[1]. Concomitant with these changes are alterations in endocrine states, such as decreased sex hormone production, and reduced growth hormone and insulin-like growth factor-I[5]. Endocrine function and homeostatic processes, such as energy homeostasis[6] and release of sex hormones[7], are controlled by neuropeptidergic neurons in the hypothalamus.

Nutrient sensing is one of several functions of the hypothalamus that implicates this brain region in healthy aging. Specific neuronal subtypes in the hypothalamus respond to circulating cues to organize the response to dietary changes through regulation of energy balance, glucose homeostasis and growth factor secretion. Caloric restriction (CR) is one of the most well-established behavioral interventions that improves lifespan and healthspan in many model organisms[8]. Genetic models that mimic the effects of CR via modulation of energy sensing pathways have revealed the mechanistic underpinnings of lifespan extension. For example, in *C. elegans*, the effects of dietary restriction are dependent on the function of neuropeptidergic energy sensing neurons; genetic manipulation of energy sensing genes in those neurons is sufficient to increase longevity[9]. Similarly, lifespan extension in the fruit fly *Drosophila* is dependent on specialized neurons called median neurosecretory cells[10]. In rodents, manipulations to the hypothalamus can also alter lifespan. Specifically, brain-specific over expression of *Sirt1*

leads to alterations in the dorsomedial and lateral hypothalamus and increases lifespan[11]. Similarly, alteration of immune signaling in the mediobasal hypothalamus affects longevity, where a reduction in immune signaling promotes longevity[12].

Epigenetic and transcriptional changes are widespread across tissues during aging, including in the brain[13,14]. Key transcriptional factors such as FOXO/DAF-16, NF-κB,, and MYC function as conserved regulators of these networks and have been implicated in aging[12,15,16]. However, despite a great interest in how changes in transcriptional programs affect aging, our understanding of how distinct cellular subtypes change transcriptionally with age remains limited. Investigation of how transcriptional programs change in a cell-type specific manner in the hypothalamus will provide important insight into the aging process across tissues. Recent advances in single-cell RNA-sequencing (RNA-seq) have expanded our understanding of the diverse cell types that comprise the hypothalamus[17–21]. This approach allows the investigation of previously unappreciated transcriptional and functional diversity of this brain region. Here, we use a single nuclei RNA-seq approach to identify aging-associated transcriptional changes across the mouse hypothalamus, thereby capturing the diversity of cell types in this brain region.

## RESULTS

### Single nuclei sequencing of the aging mouse hypothalamus

We employed single nuclei RNA sequencing (snRNA-seq), which is currently the optimal method for single cell transcriptomic profiling of the diversity of cell types in the adult mammalian brain[22,23]. We isolated nuclei from the hypothalamus of young (3 month) and aged (24 month) mice, with replicate libraries for each age (Figure 1A). After quality filtering, we

obtained 22,718 high quality nuclei for analysis: 7862 and 14,856 nuclei from young and aged animals, respectively (Figure S1A). We observed a high correlation between replicates at each age (Figure S1B).

Clustering analysis with the Louvain algorithm revealed distinct clusters representing the major cell types of the hypothalamus, which we identified based on expression of canonical markers (Figure 1B-D, S1C). For each individual cluster, we identified the top 10 genes that were differentially expressed using the Wilcoxon Rank Sum test (Supplementary Table 1). For example, neurons were defined by expression of *Syt1*, astrocytes defined by *Agt and Gja1*, oligodendrocytes by *Olig1* and *Plp1* expression, and OPCs were identified by expression of *Pdgfra*. The microglia/macrophage cluster was defined by expression of *C1qa* (Figure 1C). Less abundant cell types were also observed, including ependymocytes (ependymal cells; *Ccdc153*), and arachnoid barrier cells (ABC; *Slc47a1*), pericyte/endocytes (*Flt1* and *Clnd5I*) and vascular and leptomeningeal cells (VLMC; *Slc6a13*). We also observed a distinct cluster of tanycytes, which are specific to the hypothalamus and defined by *Rax* expression. Nuclei in these broad categories expressed additional canonical markers associated with their cell type, for example, the astrocyte cluster expressed *Gfap,* further validating the identify of each cluster.

Cell type diversity is achieved through expression of transcriptional regulators that orchestrate cell type-specific gene expression networks. To identify the regulators responsible for distinct expression networks across cell types in the hypothalamus, we used SCENIC, a regulatory network inference tool. This analysis revealed specific transcriptional regulators of cell identity in this region[24] (Figure 2). Strong cell-type specific signatures emerged for each

cluster. Some regulons, such as Foxn2, are strongly enriched across all cell types, while others are unique to one or two cell types. For example, Atf2 is uniquely highly enriched in neurons. In tanycytes, a cell population unique to the hypothalamus, the regulons Foxo1 and Foxo3 are enriched. Tanycytes are considered to be neurogenic, and function in response diet[25,26]. FOXO factors are critical regulators of neural stem cell homeostasis, and FOXOs sit downstream of the insulin/IGF-1 pathway[27]. These data suggest that FOXO factors may be critical regulators of tanycyte response to organismal energy states.

**Major cell types of the hypothalamus acquire cell type-specific gene expression changes with age**

We next investigated the changes in gene expression that occur with age in the major cell types of the hypothalamus. As expected, aging was not associated with changes in composition of this brain region, and each major cell type was similarly represented in young and aged mice (Figure 3A). To control for differences in nuclei numbers obtained, we randomly downsampled the aged nuclei and performed differential expression analysis on identical numbers of aged and young nuclei (Figure S2A-C). To gain a global understanding of how gene expression is altered with age, we first performed differential expression analysis using the Model-based Analysis of Single-cell Transcriptomics (MAST)[28,29], treating the data in bulk. Using this approach, we identified 216 and 326 genes that were upregulated and downregulated with age, respectively (padj < 0.05, fold change > 0.1) (Figure 3B, Supplementary Table 3). Intriguingly, highly downregulated genes included *Pmch* and *Oxt*, which encode Pro-melanocyte stimulating hormone and Oxytocin, respectively. Melanocyte stimulating hormone and oxytocin are heavily involved in regulating energy homeostasis[6], which is altered with age[30]. Interestingly, the most

upregulated genes included *Xist* and *Tsix*, which are both long non-coding RNAs involved in X chromosome inactivation[31,32].

Next, we investigated the impact of age on gene expression in each major cell type. Neurons, astrocytes, oligodendrocytes, and microglia showed the greatest numbers of differentially expressed genes with age (Figure 3C, Supplementary Table 4). Analysis of most other cell types also revealed differential expression, though the ability to discern differentially expressed genes was related to the number of nuclei per cluster (Figure S2D). We also performed coefficient of variation analysis on the major cell types and, interestingly, we observed a significant difference between ages, with nearly all types showing in increase with age ($p < 0.001$; Wilcoxen test) (Figure 3D). This finding suggests that variability in gene expression increases with age in each cell type, which likely contributes to cellular dysfunction with age.

To investigate the cellular processes that are altered with age in the different cell types in the hypothalamus, we performed Gene Set Enrichment Analysis (GSEA) using the hallmark gene set[33] (Figure 3E). Interestingly, the neuron sub-cluster had the greatest number of gene sets represented, which included a number of known aging-associated pathways. For example, metabolic pathways such as PI3K/AKT/mTOR, adipogenesis, glycolysis and OxPhos were all under-enriched with age (negative normalized enrichment score). In addition, DNA damage and repair pathways, p53 signaling, and proteostasis were all downregulated in the aged neurons. This analysis also revealed a number of cell type-specific changes with age. For example, among the pathways that were altered with age in astrocytes, some overlapped with the neuronal

changes (e.g unfolded protein response and mTORC1 signaling) while others were specific to glia (e.g. coagulation factors, the inflammatory response and NFKB activity).

**Aged hypothalamic microglia are heterogeneous, representing a progressive aging trajectory**

Microglia are macrophage-like cells found throughout the brain, and are critical for the immune response, including release of cytokines and chemokines, antigen presentation, and phagocytosis of debris[34]. Recent studies have revealed gene expression changes and microglial activation in the aged brain, which likely contribute to neurodegeneration[34]. Due to the lower frequency of microglia in our dataset, we sought additional strategies to uncover changes with age in these cells. Using Monocle3[35], we performed pseudotemporal ordering of the microglia/macrophage nuclei. The trajectory accurately captures the transition from young to aged nuclei, suggesting a gradual progression toward aging in this cell type (Figure 4A). To identify the gene expression changes across the aging trajectory, we performed Moran's I test (Figure 4B, Supplementary Table 5, Supplementary Table 6). This approach revealed four modules (1, 2, 3, and 7) that have decreased expression along the pseudotime trajectory, and three modules (4-6) with increased expression (Figure 4B-C). We named modules after their most enriched GO term. The modules decreasing in expression along the pseudotime trajectory include terms related to neurotransmitter release, cell migration, cell projection and cytoskeleton makeup, and myelination (Supplementary Table 6). In contrast, the modules increasing with expression across pseudotime include immune response, regulation of cell-cell signaling, and response to immune signals (Supplementary Table 6).

To gain a deeper understanding of the heterogeneity of microglial aging in the hypothalamus, we examined the top 20 most significant genes for each cluster (q value < 0.05). We visualized expression of genes with high significance in the module and plotted gene expression as a function of pseudotime, and directly comparing young and aged populations (real-time; Figure 4D). This approach reveals that while the young microglia are clustered early in pseudotime (pseudotime 0.0, 0.5 and 1.0), microglial nuclei from aged animals are dispersed throughout pseudotime. Indeed, pseudotime 1.5 and 2.0 are comprised almost entirely of nuclei from aged animals, and expression in these cells varies strongly compared to expression in cells in pseudotime 0.0. Thus, hypothalamic microglia from aged animals have increased heterogeneity representing a progressive aging trajectory, with a subset of microglia retaining a youthful gene expression signature.

**Age-associated changes in X-inactivation genes is a sexually dimorphic feature of aging**

Sex differences in lifespan have been documented in many species, including mice[36]. In addition, interventions that extend life span do so in a sex-specific manner. For example, caloric restriction (CR) is one of the most robustly studied interventions and its effects have been observed from yeast to non-human primates[8]. Like many interventions, CR has sex-specific effects, with restricted females generally living longer than males on the same diet[37,38]. Similarly, the brain-specific *Sirt1* overexpression model results in a larger lifespan increase for females when compared to males[11]. To understand how the female hypothalamus may be uniquely affected by aging, we used female animals in our study.

Our initial differential expression analysis revealed the unexpected finding that the long non-coding RNA *Xist* is the most highly upregulated gene in the female hypothalamus with age (Figure 3B). Differential expression analysis of each major cell type indicated upregulation of *Xist* with age in astrocytes, neurons, oligodendrocytes, as well as tanycytes (Figure 5A). *Xist* is involved in X chromosome inactivation in females and is encoded on the X-inactivation center (XIC), which harbors additional non-coding RNA genes involved in the same process[39]. Intriguingly, we observed age-related upregulation of two of these RNAs in some cell types: *Tsix* and *Ftx*[40] (Figure 5A). We validated the upregulation of *Xist* using whole cell RNA preps from the hypothalamus and investigated other brain regions as well (cerebellum, cortex and olfactory bulb). All regions trended toward increased expression of *Xist* with age, but the strongest upregulation was observed in the hypothalamus (Figure 5B). As expected, we did not detect *Xist* expression in adult male mice, and there was no upregulation of this gene with age in males (Figure 5B).

The age-associated dysregulation of XIC genes lead us to investigate whether there was an enrichment for expression changes among genes on the X chromosome. Because all three XIC genes assessed were differentially expressed with age in the neuronal cluster (Figure 5A), we focused on neurons. Interestingly, a chi-square analysis indicated that the proportion of upregulated and downregulated genes was not distributed as expected between the X chromosome and autosomes ($X^2 = 8.7548$, df = 2, p-value = 0.01256). There were more downregulated genes arising from the X chromosome than expected (24 observed, 13.732428 expected, standardized residual = 2.9107035). Additionally, there were fewer nonsignificant genes than expected (198 observed, 209.292371 expected, standardized residual = -2.6499813)

(Figure 5C). Since the function of *Xist* is to silence gene expression in *cis* on the X, this observation suggests that increased *Xist* with age may contribute to the repression of expression with age across the chromosome.

Although most genes on the inactive X chromosome are not expressed in females, a small number of genes are well-known to "escape" inactivation, and are expressed from both X chromosomes. In the mouse brain, 14 genes are considered to be X escape genes not silenced by the XIC[41]. This list includes both *Xist* and *Ftx*, which have increased expression with age in our dataset. To determine if increased XIC gene expression with age might be affecting escape genes, we interrogated expression of the other 12 genes in this category. We found that most escape genes were not significantly altered with age in our dataset. In contrast, the X escape genes *Syp* and *Plp1* have decreased expression with age in neurons and oligodendrocytes, respectively. *Ddx3x*, a gene involved in neurodevelopment, showed significantly increased expression with age in astrocytes, although it appears to be expressed at low levels overall (Figure 5D). Together, these data indicate the effect of XIC gene alterations with age may be cell-type specific, and that increased *Xist* expression does not exclusively correlate with the X escape network.

**Neuronal subtype specific changes during aging**

Hypothalamic neurons are highly diverse and function to orchestrate a wide range of processes and behaviors necessary for organismal survival[42]. This diversity of function is accomplished by cell type-specific gene expression programs, with each area of the hypothalamus containing a range of transcriptionally dissimilar neuronal subtypes[17,18,21]. Indeed,

even neurons expressing the same neuropeptide gene may comprise functionally distinct subpopulations[43]. To address this complexity, we sub-clustered the neuronal nuclei to identify transcriptionally distinct populations. This analysis revealed 34 transcriptionally distinct clusters (Figure 6A), and broadly separated the nuclei into inhibitory (*Gad1* expressing GABAergic) or excitatory (*Slc17a6* expressing glutamatergic) identity (Figure 6B). The 34 clusters represent both known and undefined neuronal subtypes (see Supplementary Table 7 for markers of cluster identity). To discern the relationship between the clusters, we organized them according to transcriptional similarity using a Cluster Tree analysis (Figure 6C). Neuronal subpopulations from the same hypothalamic nucleus were not necessarily transcriptional neighbors on the cluster tree. For example, even though some AgRP/NPY neurons and POMC neurons may arise from common progenitors[43], the Npy/Agrp (23) and Pomc/Tac2 (25) clusters are not most closely related to one another.

We next investigated expression of specific neuropeptide genes across the clusters in order to functionally define the distinct neuronal subpopulations (Figure 6D). These clusters generally correspond to known cell types expressing one or two hallmark neuropeptides. As additional insight into neuronal subtype identity, we utilized the SCENIC pipeline to uncover regulons enriched in each cluster[24] (Figure 6E, Supplementary Table 8). For example, Tbx3 is a known regulator of Npy/Agrp cluster (23), and the Tbx3 regulon is active in this cluster in our dataset[44]. Similarly, both POMC and AgRP/NPY neurons are leptin-responsive, and Stat3, the transcriptional regulator of leptin response, is active in both these populations.

Using this approach, we were able to associate many of these clusters with a known function and location in the hypothalamus, as well as specific changes with age. Similar to our analysis of the whole hypothalamus, we did not detect major changes in neuronal composition with age (Figure 7A). We next performed differential expression on clusters in which there were at least 20 nuclei per condition (Figure 7B, Supplementary Table 9). The number of differentially expressed genes appears to be a function of the number of nuclei per cluster, for example, the Npas3/Gpc cluster (12) which has a large number of nuclei (1923) shows 224 genes downregulated in age and 70 genes upregulated in age. For each cluster, we also performed GSEA using the Hallmark gene set. Interestingly, several neuronal subtypes involved in feeding and energy homeostasis were altered with age. For example, *Ralyl* and *Tenm2* were upregulated in the Npy/Agrp cluster (23). In the Pomc/Tac2 cluster (25), *Plod1* and *Cxcl12* were downregulated, and *Epha6, Xist, B3galt1, Lingo2*, and *Sgcz* were upregulated. Pathways altered in this cluster with age include adipogenesis, DNA repair, oxidative phosphorylation, the unfolded protein response, and UV response down (Figure 7C). Thus, for the first time, our dataset links neuron-specific gene expression changes in the hypothalamus with key features of organismal aging, such as weight and metabolic changes.

Based on expression of specific peptides and transcription factors, the Dgkb/B230323A14Rik cluster (7) is likely made up of cells of the medial mammillary nucleus. This region is notable because unlike most areas of the hypothalamus, this region is involved in memory via connections with the hippocampus[45]. Strikingly, this cluster is highly dysregulated with age, with 65 downregulated and 31 upregulated genes. This gene set is enriched for changes in adipogenesis, mTORC1 signaling, OxPhos, DNA damage (UV response down), and

293 xenobiotic metabolism. The identification of changes in this brain region is significant, as they
294 may contribute to cognitive impairments with age.

295 **DISCUSSION**

296 In this work, we used single nuclei RNA-seq to identify the age-associated transcriptional
297 changes in the mouse hypothalamus. This brain region is critical for the regulation of
298 physiological homeostasis, including sleep, circadian rhythms, feeding, and metabolism. These
299 functions are well known to be disrupted during aging, and our findings implicate widespread
300 transcriptional changes concomitant with physiological changes.
301
302 Our approach successfully captured the major cell types in the brain, as well as
303 hypothalamus-specific cell-types such as tanycytes. We found that cellular subtypes in this
304 region acquire distinct aging signatures, and discovered that increased transcriptional
305 heterogeneity is a common feature across all cell types with age. Consistent with our findings,
306 age-related transcriptional alterations have been observed in aging human brains[46], and increased
307 transcriptional noise is thought to be a hallmark of aging[47]. Our finding that different neuronal
308 subtypes have distinct aging signatures is consistent with recent reports identifying differential
309 susceptibility to neurodegeneration[48]. Identification of the transcriptional signatures involved
310 may pave the way for therapeutics targeted at subpopulations most susceptible to dysregulation
311 with age. In addition, analysis of cell types arising from the arcuate nucleus illustrate intriguing
312 cell-type specific differences in populations responsible for nutrient sensing. For example,
313 despite the importance of AgRP/NPY neurons in initiating feeding in steady state animals[49], the
314 Npy/Agrp cluster (23) is relatively unaffected by age. In contrast, the Pomc/Tac2 cluster (25)
315 gene set is enriched for changes in DNA repair and the unfolded protein response, among others.

316 While these two cell populations have complementary functions in steady state, POMC neurons
317 seem to be uniquely affected by aging. Interestingly, upregulation of the unfolded protein
318 response has been linked to improved protection against diet-induced obesity[50]. Thus, the
319 downregulation of the unfolded protein response pathway with age in these cells may represent a
320 mechanism underlying body composition changes that occur with age.
321
322 We observed striking changes in the microglial population with age. Microglia are
323 resident immune cells in the brain, and previous research has shown that microglia-mediated
324 inflammation in the hypothalamus can affect lifespan[12]. By utilizing trajectory inference
325 analysis, we uncovered an aging trajectory among microglia in the aged brain. While some
326 microglia retain features of young cells, the population shows a progression toward an aged
327 phenotype based on distinct gene expression modules. Interestingly, modules of immune genes
328 were some of the most changed throughout pseudotime. Module 2, which contains GO
329 categories related to leukocyte migration, cell chemotaxis, and cell-cell adhesion, was among the
330 most downregulated with pesudeotime. In contrast, Module 4, which also contains GO categories
331 related to immune function, was highly upregulated with pseudotime. Together, these data
332 indicate that the aged hypothalamus harbors a heterogeneous population of microglia comprising
333 an aging trajectory.
334
335 Sex differences in aging have been observed across taxa, including in mice[51,52]. In
336 mammals, females generally live longer than males[53], and many aging interventions such as CR,
337 are more effective in females[11,37]. In addition, the sexually dimorphic response to aging
338 interventions appears to be a conserved phenomenon, with female *Drosophila* responding more

339 strongly to dietary restriction paradigms than males[54], and hermaphroditic *C. elegans* responding
340 more strongly to DR than males[55]. In mice, males and females differ in regards to sex
341 chromosome content (males are XY and females are XX) and the presence of gonadal hormones
342 such as higher androgens in males and estrogens in females. Interestingly, X chromosome
343 content has been linked to longevity, and the presence of two X chromosome contributes to
344 increased longevity regardless of hormonal status[56]. This work was performed in the four core
345 genomes mouse line, in which the *Sry* gene (which induced testes development) exists on an
346 autosome rather than the Y chromosome, allowing for chromosomal sex to be disambiguated
347 from gonadal sex/hormone status. In our study, we uncover a potential mechanism by which the
348 X chromosome affects aging. We observed widespread upregulation of *Xist* in aged female
349 animals, as well as upregulation of other XIC genes including *Tsix* and *Ftx*. Intriguingly, this
350 increased expression was highly prominent in neurons, although upregulation of *Xist* in was
351 observed in oligodendrocytes, astrocytes, and tanycytes as well. Together, our findings reveal a
352 novel feature of aging in females. Moreover, this work suggests that that understanding the
353 mechanisms and consequences of *Xist* upregulation in aging may provide novel insight into sex
354 differences in aging.
355
356 In summary, our study reveals the major transcriptional features of hypothalamic aging.
357 We observed transcriptional variation across cell types, cell-type specific aging signatures, and
358 novel features of aging in females. Understanding how individual populations of cells in this
359 region contribute to overall loss of homeostasis with age will be vital to identifying treatments
360 for aging and age-related disease.
361

## METHODS

*Animals*

Young (3 month) and aged (24 month) C57/Bl6 female mice were obtained from the National Institute on Aging. Mice were housed and used according to protocols approved by Brown University and in accordance with institutional and national guidelines.

*Single-cell RNA sequencing*

Two whole hypothalamuses were pooled into each biological replicate, for a total of two replicates for the young and aged conditions. Nuclei extraction was performing using the Nuclei Isolation Kit: Nuclei PURE Prep Kit (Millipore Sigma) according to the manufacturer's instructions with the following modifications: for each sample, two hypothalamuses were dissected out of the animals and rinsed in cold PBS. Tissue was transferred using a transfer pipette into a refrigerated Dounce homogenizer with 5 mL of lysis solution following kit instructions. Tissue was homogenized with the Dounce B and the lysate was transferred into a 15 mL falcon tube through a 40-micron filter. The sucrose purification step was performed with the following modifications: half the volume of all reagents was used to account for the small tissue sample sizes, an SW34 rotor was used, and samples were spun for 45 minutes at 30,000 X g (13,000 rpm) at 4 °C. Nuclei were counted using a hemocytometer, and 5000 cells per sample were loaded onto the Chromium Single Cell 3′ Chip (10x Genomics) and processed with the Chromium Controller (10x Genomics). Libraries were prepared using the Chromium Single Cell 3′ Library & Gel Bead kit v2 according to manufacturer's instructions. Samples were sequenced at GENEWIZ, Inc on an Illumina HiSeq, with a target of 50,000 reads per sample. The Aged 1

and Young 2 samples underwent an additional round of sequencing to obtain sufficient read depth.

*Quality control, data processing and analysis*

Demultiplexing and sequence alignment to a custom pre-mRNA transcriptome (mm10-3.0.0) were performed using the CellRanger (version 3.0.2) software from 10x Genomics. The resulting feature-barcode matrices were read into R, excluding any nuclei expressing fewer than 200 genes, and any gene expressed in fewer than three nuclei.

Filtering and visualization were performed using Seurat_3.2.3 in R (4.0.3). For quality control, cells with fewer than 200 or more than 3000 features were filtered out. Similarly, cells with more than 10% mitochondrial mapping were removed, resulting in 14,856 nuclei in the aged condition, and 7862 nuclei in the young condition. Integration of the datasets was performed using the IntegrateData function with default settings. The number of cells, unique molecular identifiers, and unique genes per cluster are reported in Supplementary Figure 1C. To assign identities to clusters, the FindAllMarkers() command with default parameters was used. This finds the top genes that define a cluster identity. We named each cluster using the top 2 genes to come out of the FindAllMarkers() analysis. This function uses the Wilcoxon Rank Sum test identify the top 10 differentially expressed genes in cell-type specific clusters, with a log fold change threshold of 0.25.

In order to ensure similar cell counts per condition, data were downsampled by randomly selecting cells from each cluster using the sample() function in R. Differential expression was

408 performed using MAST(1.16.0)[28]. Genes were considered significant if the adjusted p-value was
409 less than 0.05, and the log2 fold change was greater than 0.1 or less than -0.1.
410
411 *Gene Set Enrichment Analysis*
412 Gene Set Enrichment Analysis was performed using the fgsea package (Release 3.12)[57]
413 using the Hallmark gene set list (version 7.2.)[33]. Gene sets were considered to be enriched if the
414 adjusted p value was less than 0.1. Conversions between mouse and human annotation was
415 performed using biomaRt (2.46.0).
416
417 *Trajectory inference and analysis using Monocle3*
418 The trajectory inference tool Monocle3[35] (https://github.com/cole-trapnell-lab/monocle3)
419 was used to infer the aging process for the microglia cluster (n = 761 cells) generated in Seurat.
420 The microglia cluster was subsetted and the root of the trajectory was programmatically
421 specified using the node that was most enriched with young cells. Spatially differential
422 expression analysis along the trajectory was performed with Moran's I test in Monocle3 using
423 the downsampled microglia data (n = 448 cells), and selected genes with $q < 0.05$ as trajectory-
424 dependent genes. The set of genes were grouped into seven modules using find_gene_modules()
425 to run UMAP on these genes and group them into modules by Louvain community analysis
426 (Supplementary Table 6).
427
428 *Functional enrichment analysis*
429 The g:Profiler g:GOSt tool was applied to perform the functional enrichment analysis of
430 939 genes in individual microglia modules, and to identify statistically significant enriched terms

(adjusted $p < 0.05$ with Benjamini-Hochberg correction) for individual modules (Supplementary Table 5). Seven modules were identified: Module 1 (19 terms), module 2 (25 terms), module 3 (26 terms), module 4 (202 terms), module 5 (11 terms), module 6 (13 terms), module 7 (6 terms). The 939 genes were treated as unordered queries, and statistical tests were applied in a domain scope of annotated genes, choosing terms sized from 4 to 500 genes in sources including GO molecular function, GO cellular component, GO biological process, KEGG, Reactome, and WikiPathways. The top GO biological process term was used to name individual modules.

***Single-cell gene regulatory network analysis using pySCENIC***

We performed GRN analysis with pySCENIC v0.10.4[24] using the Singularity v3.6.1 image. We first converted the Seurat object (DefaultAssay: RNA, i.e. raw counts without normalization) with loomR v0.2.1.9 and export into a loom file for the GRN inference. In the GRN inference, for the downsampled all-cell data (n=15445 cells), we filtered out genes that are detected in less than 300 cells with Scanpy v1.4.4, resulting in 11574 genes in total; for the downsampled neuron data (n= 8846 cells), we used all genes (22054 genes). We performed 100 runs on both datasets. Only regulons that recurred at least 80% were retained, along with target genes that were predicted to recur at least 80% if the regulon recurred 100 times, and all target genes for regulons that recurred between 80 and 100 times[58]. After filtering, we identified 216 motif regulons for all-cell dataset, and 285 motif regulons for neurons. The regulon activity was quantified by AUCell with AUCell_calcAUC in AUCell R package v1.8.0, R/3.6.3. To understand if a regulon is active or not in a specific cell type, we created a binary regulon activity matrix of the filtered regulons with binarize function in pyscenic.binarization and visualized in R. For the regulon specificity score (RSS), we use the regulon_specificity_scores

455 from pyscenic.rss[59]. The RSS is calculated for each cell type separately, and top 5 regions for
456 each cell type are shown in red.ref.

457
458 *Data and code availability*

459 Raw single nuclei RNA sequencing deposited at GEO accession XYZ. Code available at
460 https://github.com/Webb-Laboratory/single_cell_analysis.

461

462 *RT-qPCR*

463 Hypothalamus, olfactory bulb, cerebellum, and cortex were dissected in cold PBS from
464 the brains of 3 month old and 24 month old C57Bl/6 mice (n=6, 3 male and 3 female for each
465 age) and snap frozen in liquid nitrogen. RNA was purified using the Qiagen RNeasy Lipid
466 Tissue Mini Kit (Qiagen #74804). cDNA was generated using 500 ng of RNA and the High-
467 Capacity Reverse Transcription Kit (Applied Biosystems #4374966). A negative control (-RT)
468 for each sample was also generated by excluding the Multiscribe Reverse Transcriptase
469 component of the reaction. qPCR reactions were completed using the PowerUp™ SYBR ™
470 Green Master Mix (Invitrogen #A25918). Stock primers were diluted to 10 μM in sterile water,
471 and cDNA was diluted 1:5 in sterile water. Expression levels of the genes of interest (see table
472 below) were quantified using a ViiA 7 Real Time PCR System with QuantStudio software. *Actin*
473 was used as a housekeeping gene for normalization. Each sample, water control, and -RT control
474 sample was run in triplicate for each primer set. CT values were normalized to *Actin*, and ΔCT
475 values were plotted as $2^{-\Delta CT}$. Technical replicates were averaged per biological replicate.

476

| Gene | F sequence | R sequence |
|---|---|---|

| | | |
|---|---|---|
| *Actin* | TGTTACCAACTGGGACGACA | CTCTCAGCTGTGGTGGTGAA |
| *Xist* | GGTTCTCTCTCCAGAAGCTAGGAAG | TGGTAGATGGCATTGTGTATTATATGG |

## SUPPLEMENTARY MATERIAL

Supplementary Table 1. Markers for hypothalamic cell clusters.
Supplementary Table 2. Binarized regulons for hypothalamic cell clusters.
Supplementary Table 3. Results of differential expression analysis for all nuclei.
Supplementary Table 4. Differential expression analysis of individual cell types.
Supplementary Table 5. Results of Moran's I Test.
Supplementary Table 6. Gene modules from monocle analysis.
Supplementary Table 7. Cluster markers for neuronal subtypes.
Supplementary Table 8. Regulon specificity scores for each neuronal cluster.
Supplementary Table 9. Results of differential expression for neuronal subtypes.

Figure 1.

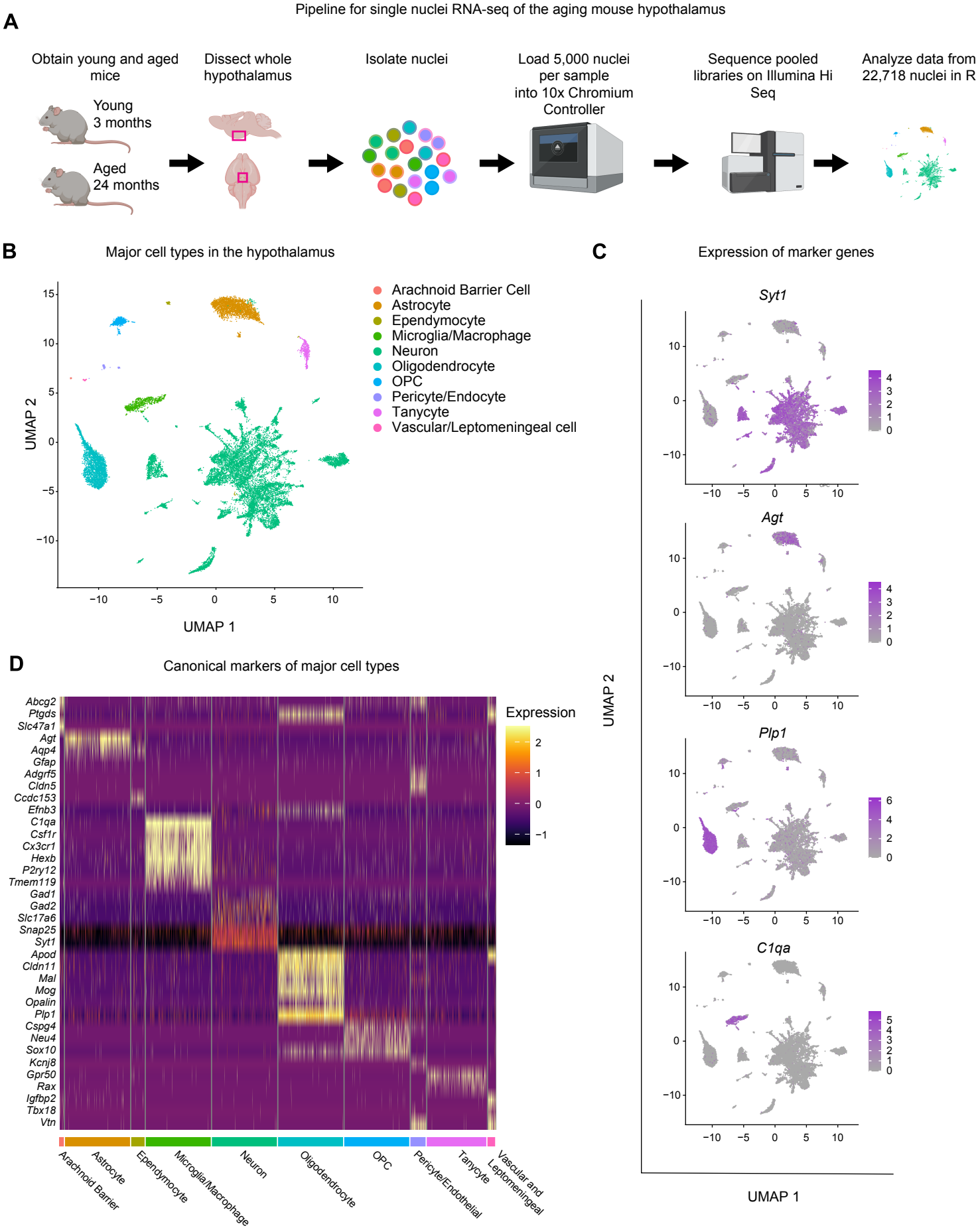

## FIGURE LEGENDS

**Figure 1. Single-nuclei analysis of the hypothalamus.** A) Schematic detailing the experimental workflow from dissection through analysis. n = 2 replicated per age. B) Uniform Manifold Approximation and Projection (UMAP) plot of all 22,718 nuclei used for analysis. Clustering analysis revealed 10 broad categories of cell type identity. C) UMAP plots of all nuclei labeled for expression of cell type-specific markers. *Syt1*, neurons; *Agt*, astrocytes; *Plp1*, oligodendrocytes; *C1qa*, microglia/macrophages. Color scale indicates level of gene expression. D) Heatmap highlighting expression of cell type markers in each cluster, a maximum of 500 nuclei per cluster are displayed. E) RSS scores for representative subclusters. Top 5 regulons in red.

Figure 2.

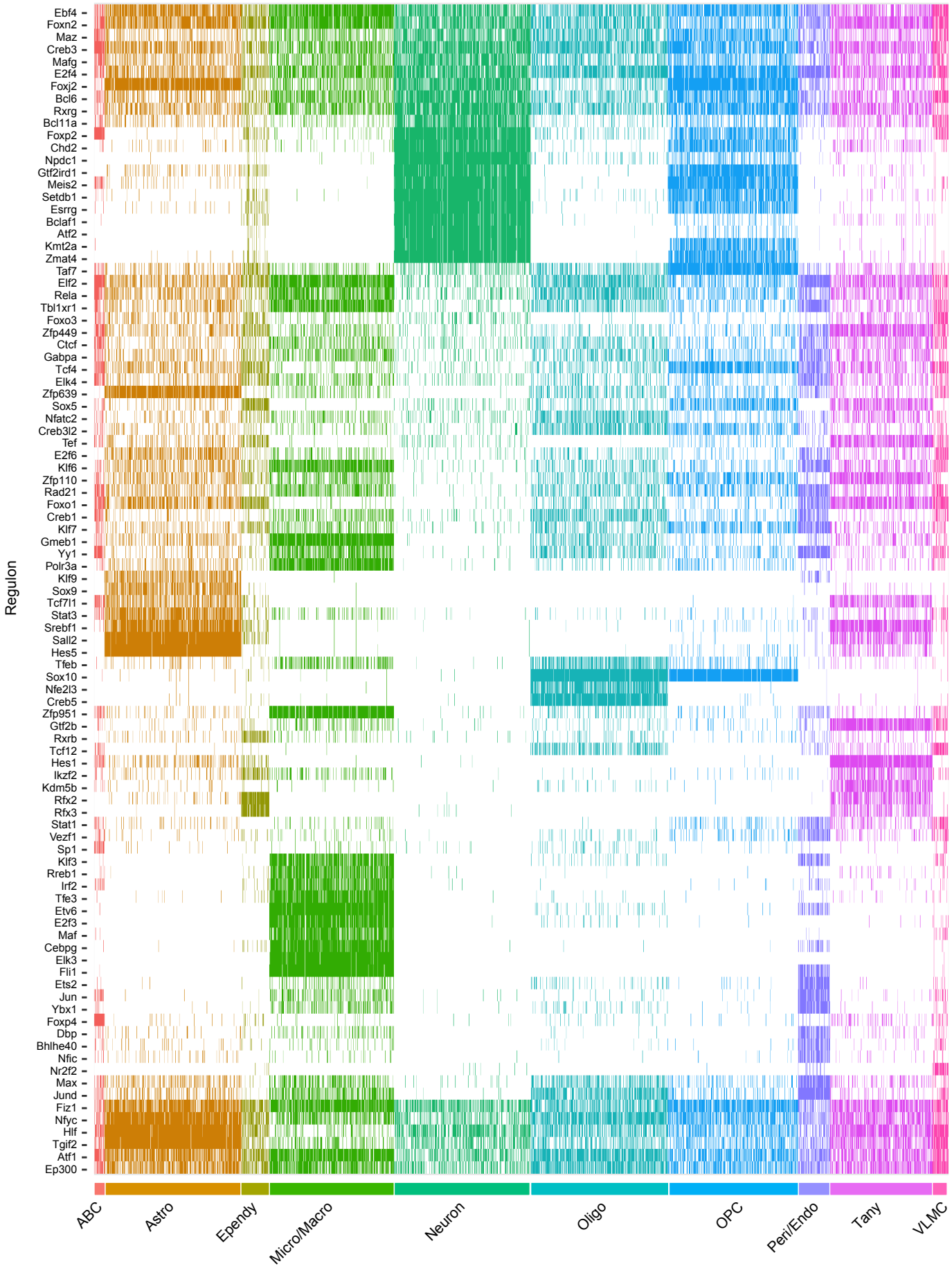

**Figure 2. Gene regulatory network reconstruction for cellular subtypes.** A) Binarized regulon activity for each regulon in a given cell. Top 20 most expressed regulons per cluster shown. Maximum 500 cells per cluster shown. Color indicates a regulon is "on" in a given cell.

Figure 3.

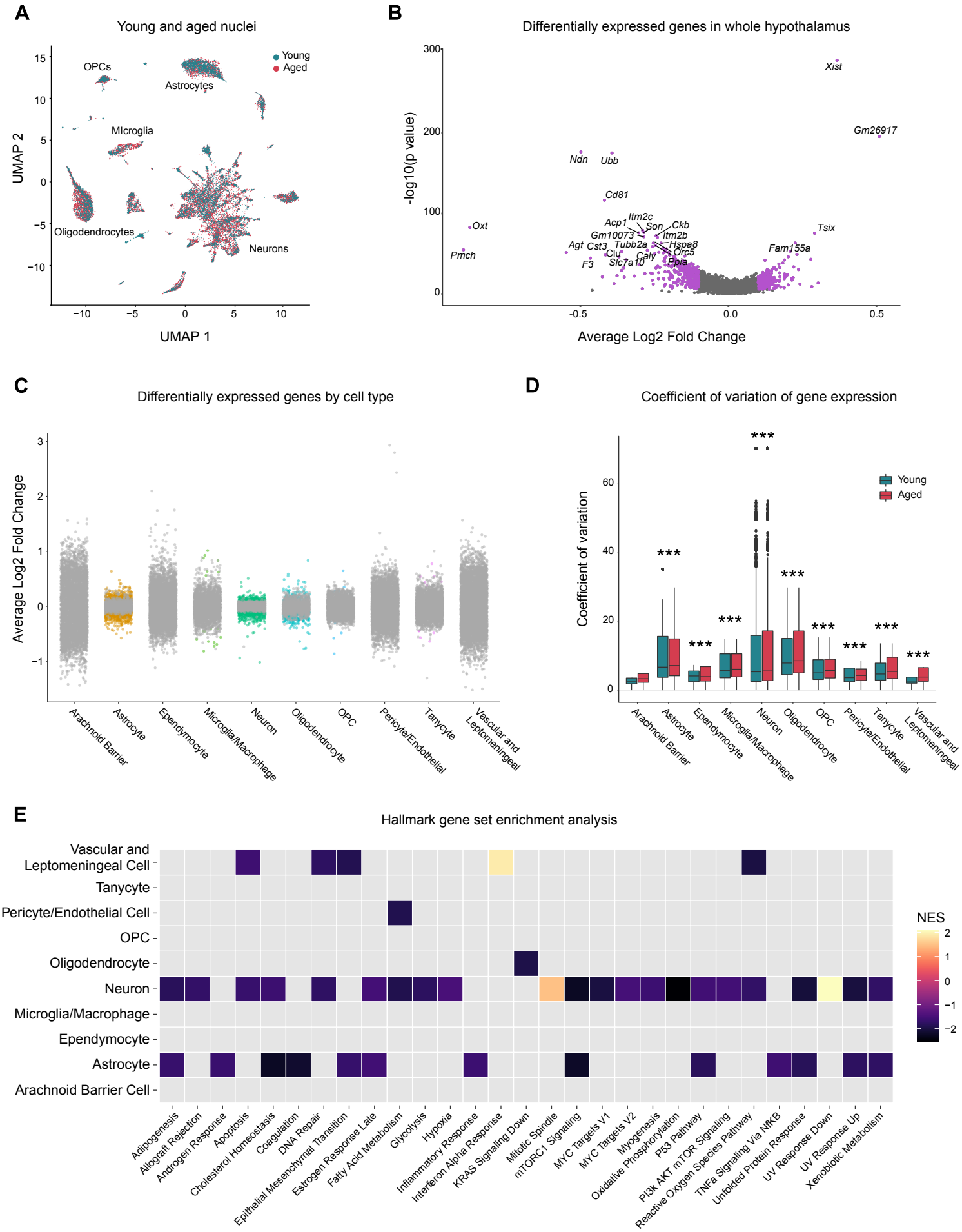

**Figure 3. The aging hypothalamus harbors cell type-specific transcriptional changes.** A) UMAP of the 22,718 nuclei analyzed, color indicates age. B) Volcano plot showing overall differential expression of genes between all young and aged nuclei. Significant genes in purple (adjusted p value < 0.05, FC > 0.1). C) Strip plot showing DE genes per cell type. Significant genes (adjusted p value < 0.05, FC > 0.1, MAST analysis) in color, nonsignificant genes are in gray. D) Coefficient of variation analysis for each cellular subtype. In all subtypes the CV is significantly higher in the aged condition (two sided Wilcoxen Test with Bonferonni correction, ***adjusted p value < 0.001). E) Heatmap showing GSEA enrichment analysis for Hallmark terms. Color indicates normalized enrichment score. Significant gene sets calculated as adjusted p value < 0.1.

Figure 4.

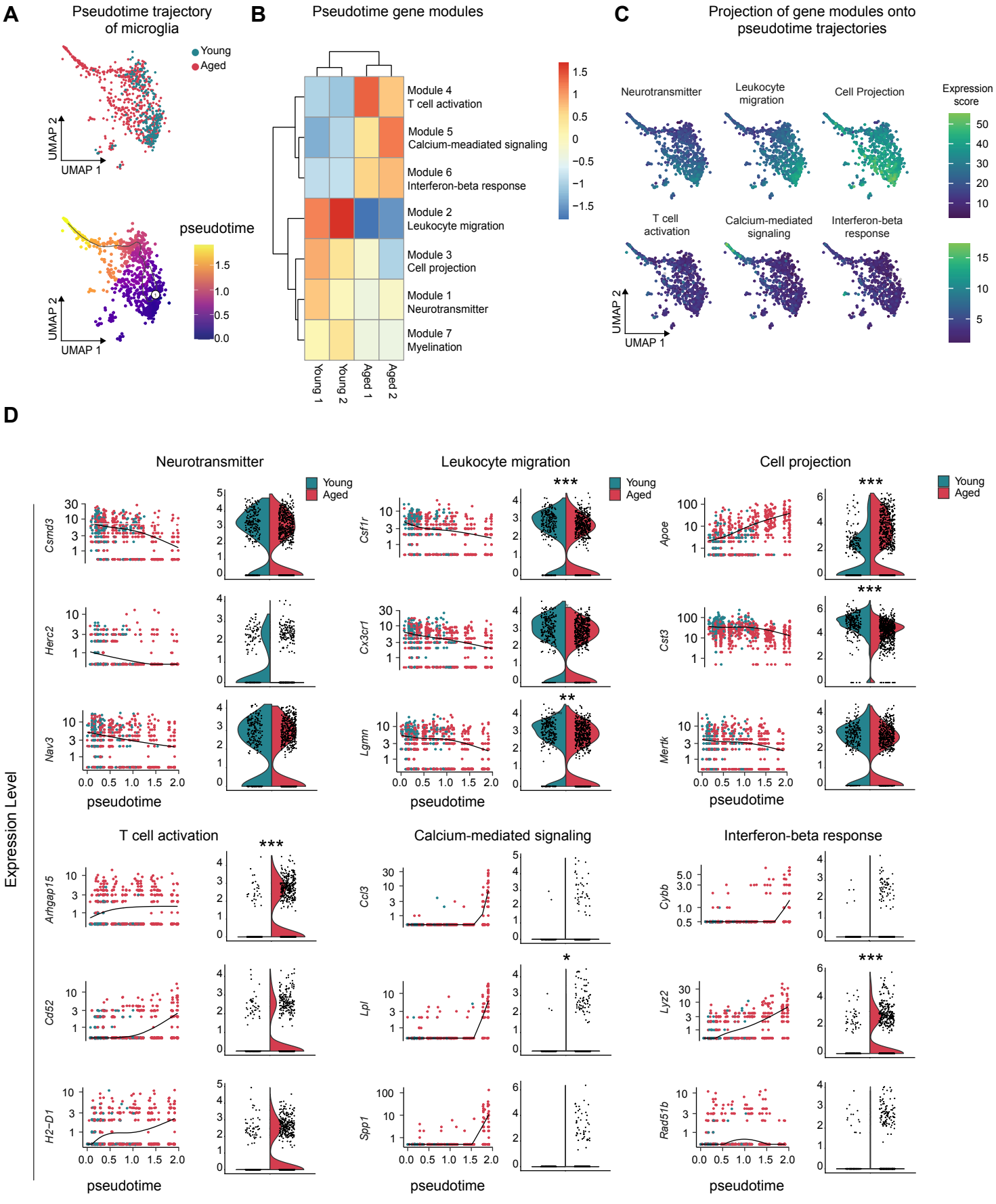

**Figure 4. Trajectory analysis of aging hypothalamic microglia.** A) Monocle3 pseudotemporal ordering of the microglia/macrophage cluster (n = 761 cells). Cells are colored by age (top) and pseudotime (bottom). The number in the circle indicates the pseudotime start point. B) Heatmap showing modules of spatially restricted genes in the microglia cluster after downsampling (n = 448 cells). In total, 939 genes were clustered by hierarchical clustering. The genes were grouped into seven modules after dimension reduction and community detection. Modules are named by the most significantly enriched Gene Ontology (GO) terms, biological process, for module-specific genes using g:Profiler (adjusted $p < 0.05$ with Benjamini-Hochberg correction). C) Projection of modules' aggregate expression onto the UMAP plot for microglia cluster (n = 761 cells). Genes in modules 1-3 have decreased expression along the pseudotime trajectory. Genes in modules 4-6 have increased expression along the pseudotime trajectory. D) Left: kinetics plot showing the relative expression of representative genes for modules 1-6. The lines approximate expression along the trajectory using polynomial regressions. Right: violin plots of gene expression using Seurat. Differential expression performed using MAST on non-downsampled data (* , adjusted p value < 0.05, ***, adjusted p value < 0.001).

Figure 5

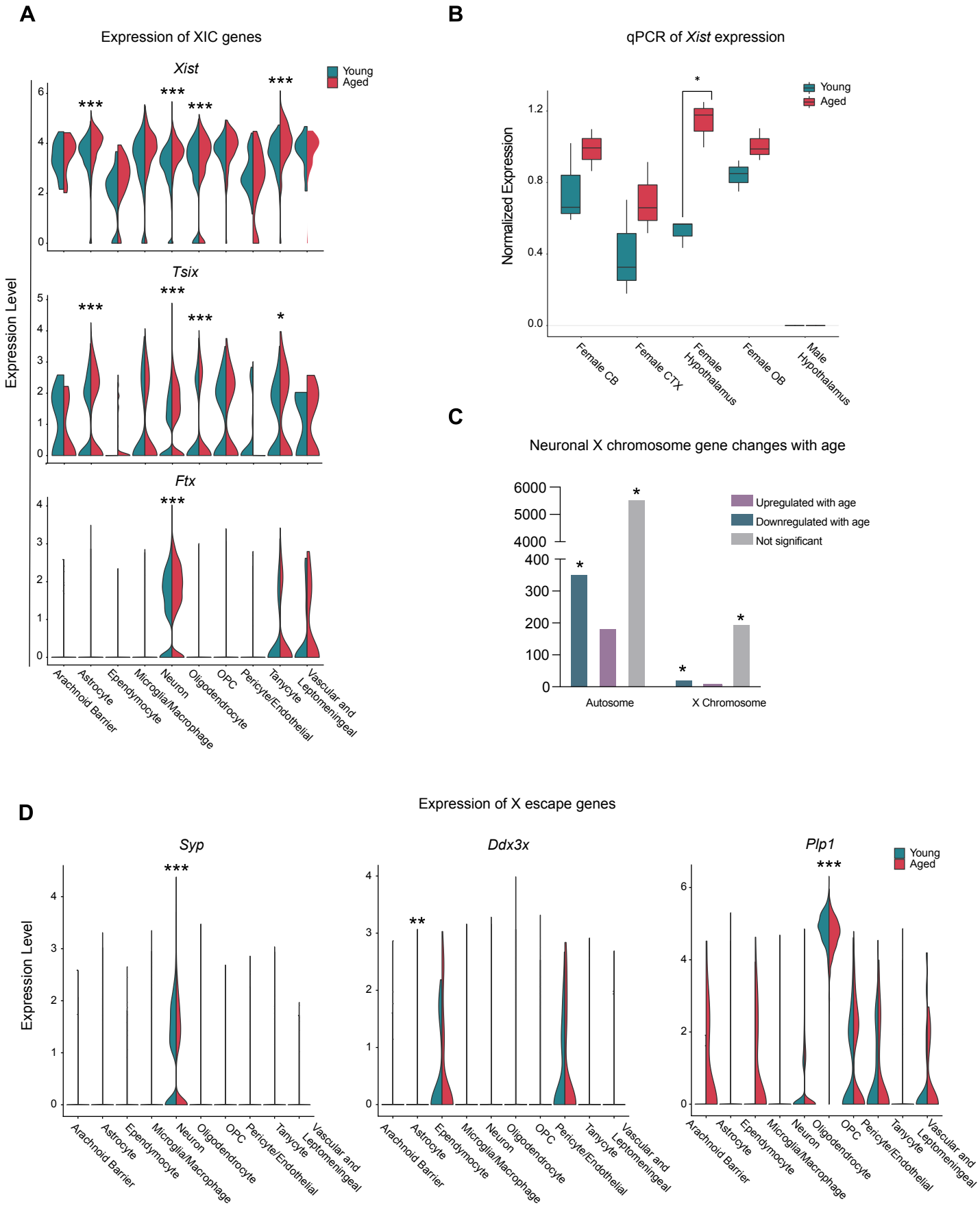

719 **Figure 5. *Xist* upregulation is a feature of the aged female hypothalamus**. A) Expression of
720 genes involved in X chromosome inactivation by age and cell type. Differential expression
721 between young and aged samples was calculated using MAST (* , adjusted p value < 0.05, ***,
722 adjusted p value < 0.001). B) RT-qPCR of *Xist* expression in specific brain regions. *Xist*
723 expression is significantly higher in the hypothalamus (two sided t test, t = 7.06, df = 3.25, n = 3
724 per age group, *p adjusted = 0.0179, Bonferroni correction). C) Comparison of the number of
725 upregulated, downregulated, and non-significant genes arising from the X chromosome or
726 autosomes in ($X^2$ = 8.7548, df = 2, p-value = 0.01256). D) Violin plots of known X escape genes.
727 Differential expression between young and aged samples was calculated using MAST (* ,
728 adjusted p value < 0.05, **, adjusted p value < 0.01, ***, adjusted p value < 0.001).
729
730
731
732
733
734
735
736
737
738
739
740

Figure 6.

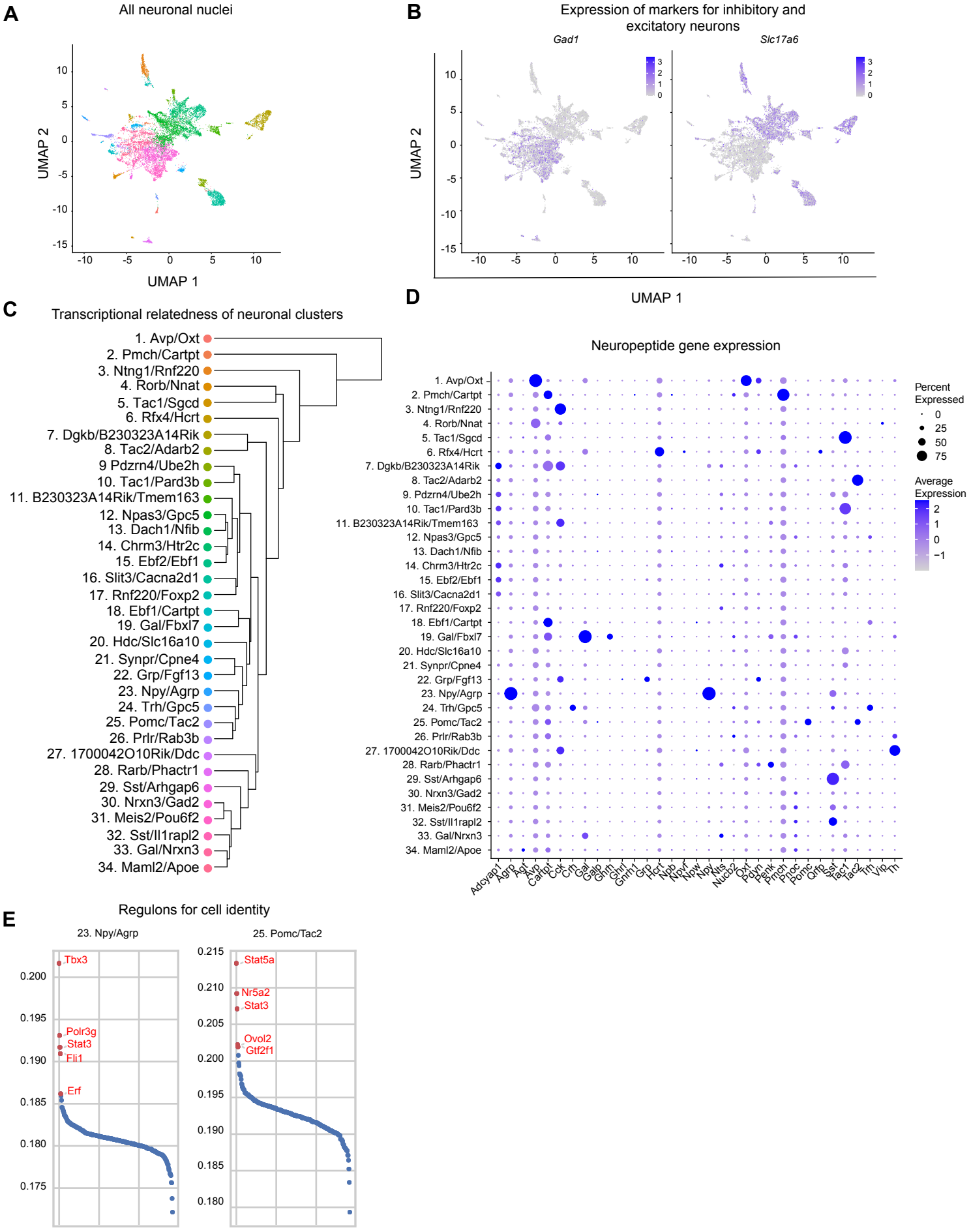

741 **Figure 6. Identification of transcriptionally distinct neuronal subtypes.** A) UMAP of all
742 neuronal nuclei. Distinct clusters are identified by color, with identities listed in (C). B)
743 FeaturePlots highlighting glutamatergic (*Slc17a6*) and GABAergic (*Gad1*) cell neuronal clusters.
744 Color scale indicates expression level. C) Neuronal clusters are labeled according to the top 2
745 marker genes and ordered based on overall transcriptional similarity. D) Expression of
746 neuropeptide genes in each cluster. Dot size indicates percent of nuclei expressing the gene,
747 color indicates intensity of expression.
748
749
750
751
752
753
754
755
756
757
758
759
760
761
762

Figure 7.

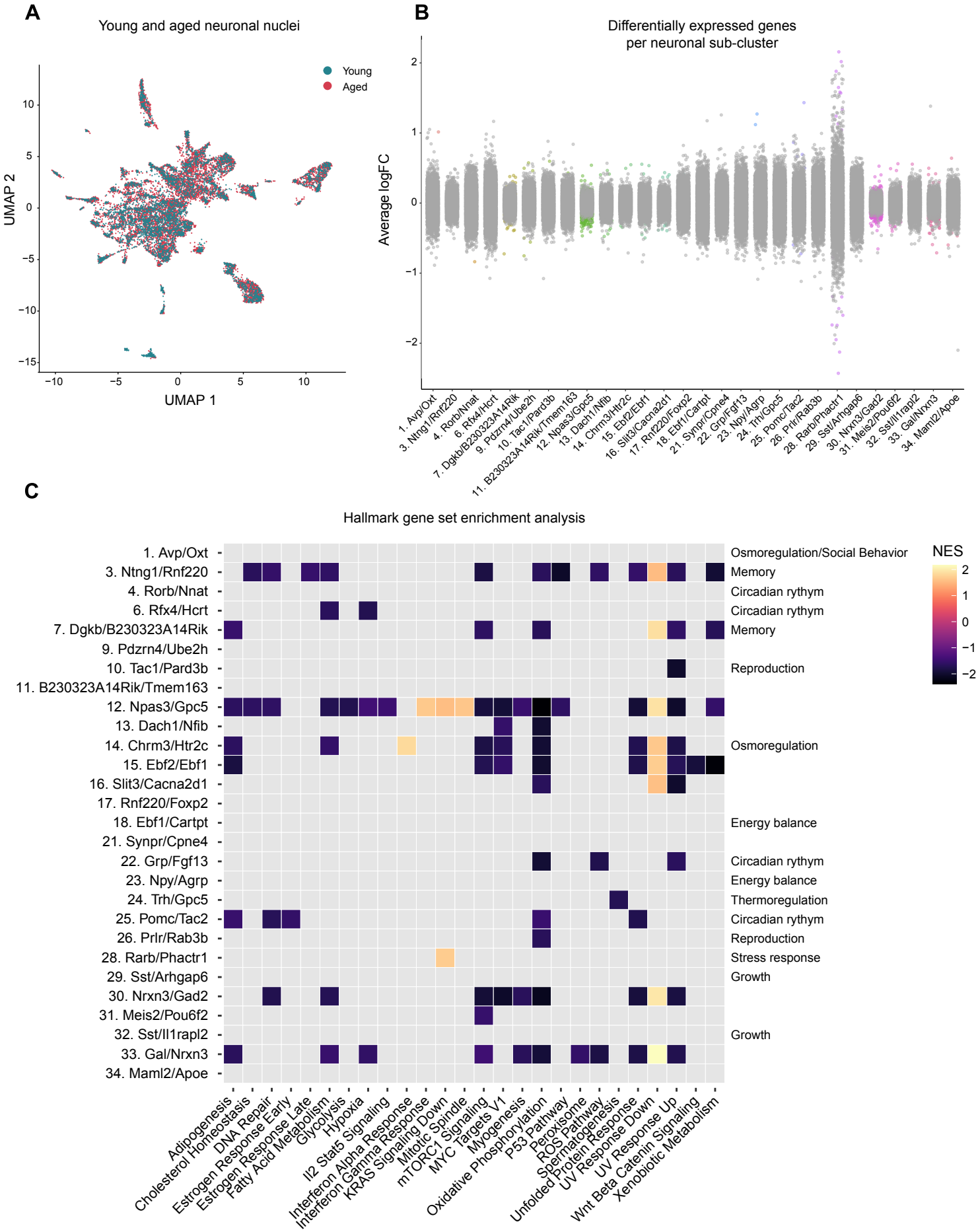

**Figure 7. Neuronal subtypes exhibit distinct transcriptional changes with age.** A) UMAP plot of young and aged nuclei. B) Strip plot showing DE genes per cluster. Significant genes (FC > 0.1, padj < 0.05) are colored, non-significant genes in gray. C) Heatmap of GSEA results for each neuronal cluster. Significantly enriched terms (padj <0.1) are colored according to the normalized enrichment score.

# Supplementary Figure 1.

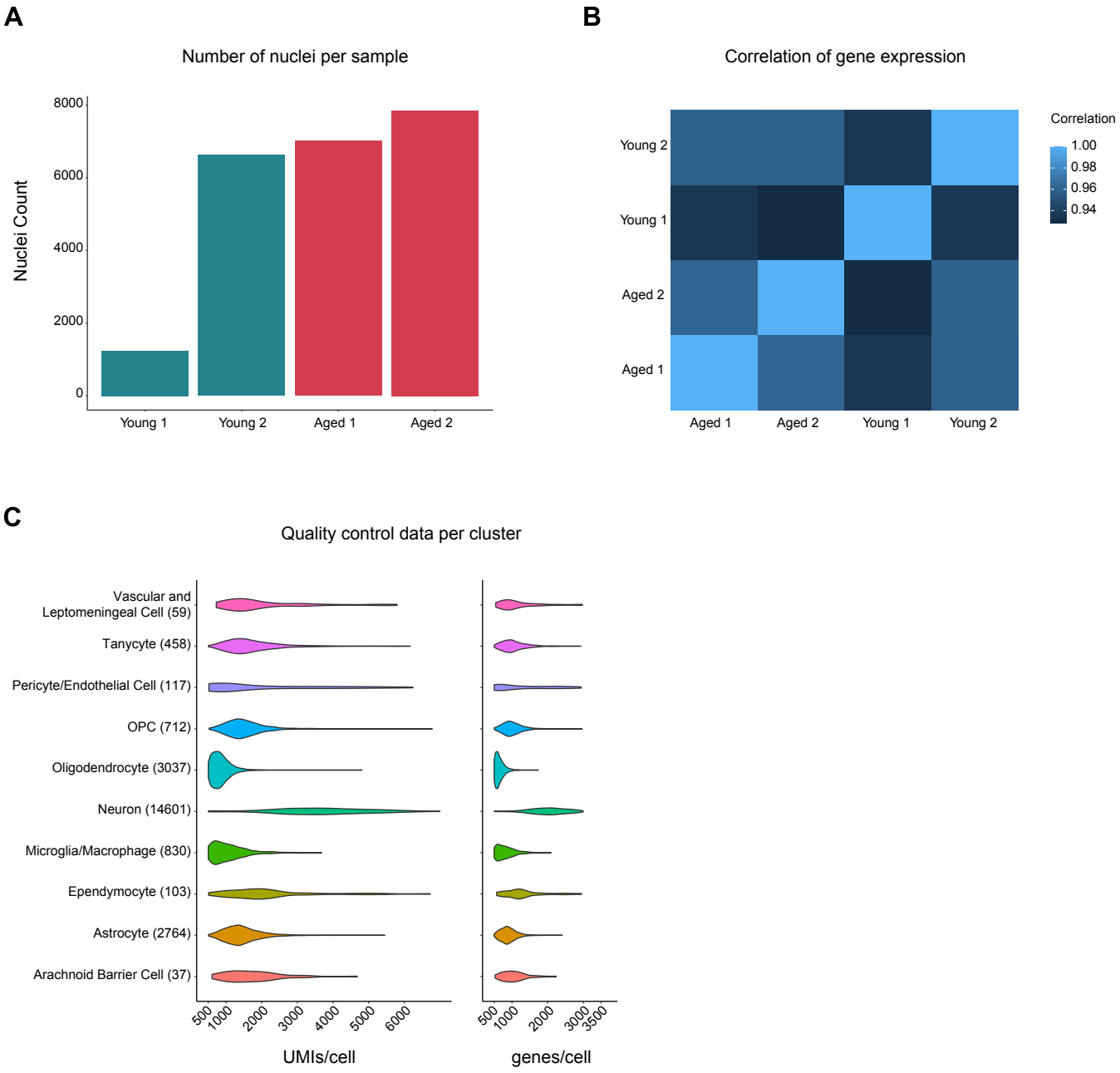

**Supplementary Figure 1**. Quality control metrics for single nuclei data. A) Number of nuclei per sample. B) Correlation of gene expression (scaled) between each sample. Color reports Spearman's correlation. C) Violin plots showing the number of UMIs per nuclei per cluster (left) and the number of genes nuclei per cluster (right). Number of nuclei per cluster are listed in parentheses.

Supplementary Figure 2.

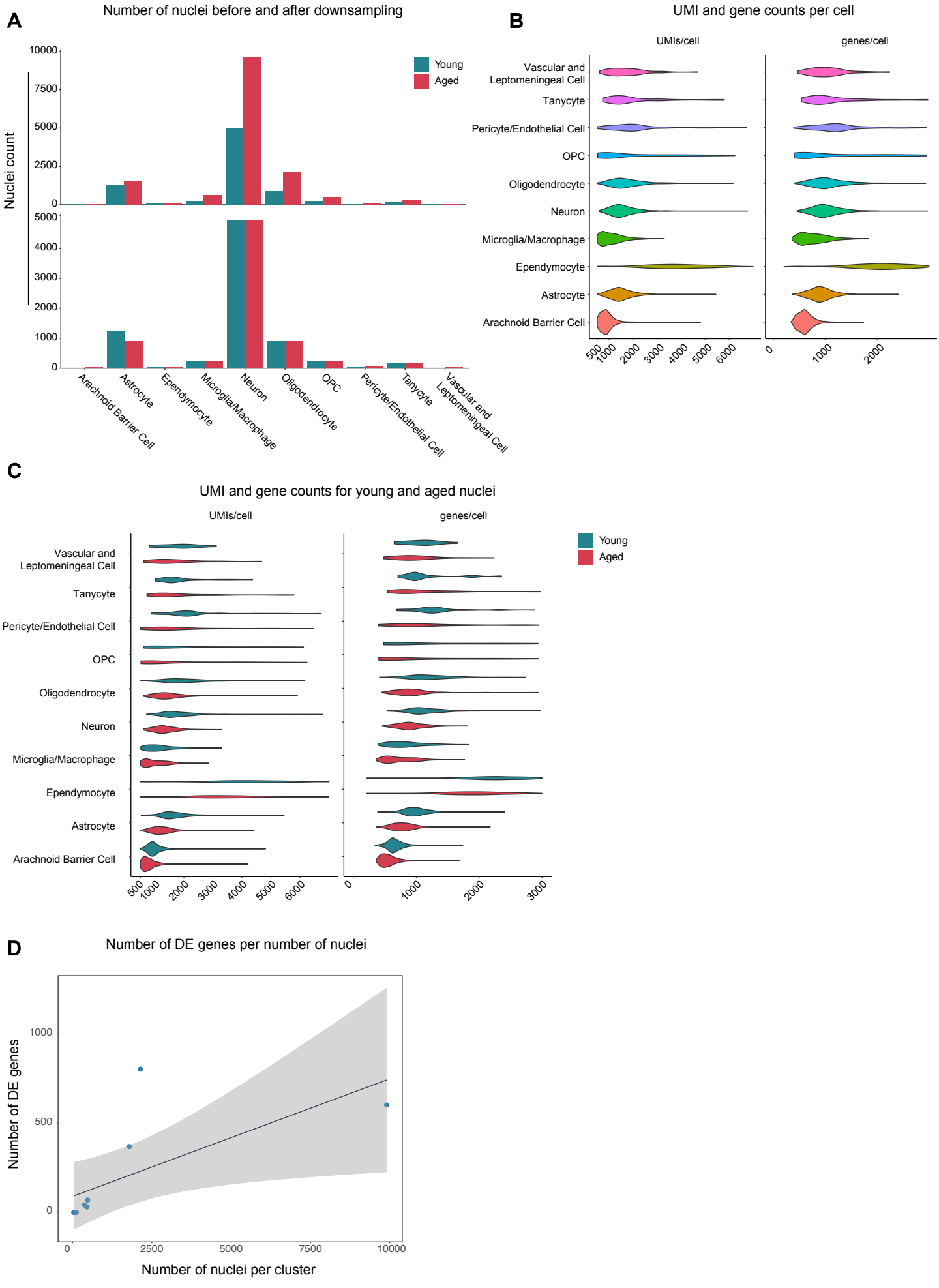

807 **Supplementary Figure 2.** Downsampling and quality control for downsampled clusters. A)
808 Number of nuclei per cell type before (top) and after (bottom) down sampling. B) Quality control
809 data for the nuclei used for analysis after down sampling. C) Quality control data after down
810 sampling split by age. D) Relationship between number of nuclei per cluster and the number of
811 differentially expressed genes. ($R2 = 0.510$ , $p < 0.05$).
812
813

## REFERENCES

1. Partridge, L., Deelen, J. & Slagboom, P. E. Facing up to the global challenges of ageing. *Nature* **561**, 45–56 (2018).
2. Yousufuddin, M. & Young, N. Aging and ischemic stroke. *Aging* **11**, 2542–2544 (2019).
3. Balducci, L. & Aapro, M. Epidemiology of Cancer and Aging. in *Biological Basis of Geriatric Oncology* 1–15 (Springer US, 2005).
4. Farooqui, T. & Farooqui, A. A. Aging: An important factor for the pathogenesis of neurodegenerative diseases. *Mech. Ageing Dev.* **130**, 203–215 (2009).
5. Chahal, H. & Drake, W. The endocrine system and ageing. *J. Pathol.* **211**, 173–180 (2007).
6. Leibowitz, S. F. & Wortley, K. E. Hypothalamic control of energy balance: different peptides, different functions. *Peptides* **25**, 473–504 (2004).
7. Hiller-Sturmhöfel, S. & Bartke, A. The Endocrine System. *Alcohol Health Res. World* **22**, 153–164 (1998).
8. de Cabo, R., Carmona-Gutierrez, D., Bernier, M., Hall, M. N. & Madeo, F. The Search for Antiaging Interventions: From Elixirs to Fasting Regimens. *Cell* **157**, 1515–1526 (2014).
9. Bishop, N. A. & Guarente, L. Two neurons mediate diet-restriction-induced longevity in C. elegans. *Nature* **447**, 545–549 (2007).
10. Broughton, S. J. *et al.* DILP-producing Median Neurosecretory Cells in the Drosophila Brain Mediate the Response of Lifespan to Dietary Restriction. *Aging Cell* **9**, 336–346 (2010).
11. Satoh, A. *et al.* Sirt1 extends life span and delays aging in mice through the regulation of Nk2 homeobox 1 in the DMH and LH. *Cell Metab.* **18**, 416–430 (2013).
12. Zhang, G. *et al.* Hypothalamic programming of systemic ageing involving IKK-β, NF-κB and GnRH. *Nature* **497**, 211–216 (2013).

13. Ximerakis, M. *et al.* Single-cell transcriptomic profiling of the aging mouse brain. *Nat. Neurosci.* **22**, 1696–1708 (2019).

14. Benayoun, B. A. *et al.* Remodeling of epigenome and transcriptome landscapes with aging in mice reveals widespread induction of inflammatory responses. *Genome Res.* **29**, 697–709 (2019).

15. Webb, A. E., Kundaje, A. & Brunet, A. Characterization of the direct targets of FOXO transcription factors throughout evolution. *Aging Cell* **15**, 673–685 (2016).

16. Hofmann, J. W. *et al.* Reduced Expression of MYC Increases Longevity and Enhances Healthspan. *Cell* **160**, 477–488 (2015).

17. Chen, R., Wu, X., Jiang, L. & Zhang, Y. Single-Cell RNA-Seq Reveals Hypothalamic Cell Diversity. *Cell Rep.* **18**, 3227–3241 (2017).

18. Mickelsen, L. E. *et al.* Single-cell transcriptomic analysis of the lateral hypothalamic area reveals molecularly distinct populations of inhibitory and excitatory neurons. *Nat. Neurosci.* **22**, 642–656 (2019).

19. Wen, S. *et al.* Spatiotemporal single-cell analysis of gene expression in the mouse suprachiasmatic nucleus. *Nat. Neurosci.* **23**, 456–467 (2020).

20. Moffitt, J. R. *et al.* Molecular, spatial, and functional single-cell profiling of the hypothalamic preoptic region. *Science* **362**, eaau5324 (2018).

21. Campbell, J. N. *et al.* A Molecular Census of Arcuate Hypothalamus and Median Eminence Cell Types. *Nat. Neurosci.* **20**, 484–496 (2017).

22. Bakken, T. E. *et al.* Single-nucleus and single-cell transcriptomes compared in matched cortical cell types. *PLOS ONE* **13**, (2018).

539 23. Ding, J. *et al.* Systematic comparison of single-cell and single-nucleus RNA-sequencing
540 methods. *Nat. Biotechnol.* **38**, 737–746 (2020).
541 24. Van de Sande, B. *et al.* A scalable SCENIC workflow for single-cell gene regulatory
542 network analysis. *Nat. Protoc.* **15**, 2247–2276 (2020).
543 25. Goodman, T. & Hajihosseini, M. K. Hypothalamic tanycytes—masters and servants of
544 metabolic, neuroendocrine, and neurogenic functions. *Front. Neurosci.* **9**, (2015).
545 26. Lee, D. A. *et al.* Tanycytes of the hypothalamic median eminence form a diet-responsive
546 neurogenic niche. *Nat. Neurosci.* **15**, 700–702 (2012).
547 27. Webb, A. E. *et al.* FOXO3 Shares Common Targets with ASCL1 Genome-wide and Inhibits
548 ASCL1-Dependent Neurogenesis. *Cell Rep.* **4**, 477–491 (2013).
549 28. Finak, G. *et al.* MAST: a flexible statistical framework for assessing transcriptional changes
550 and characterizing heterogeneity in single-cell RNA sequencing data. *Genome Biol.* **16**, 278
551 (2015).
552 29. Stuart, T. *et al.* Comprehensive Integration of Single-Cell Data. *Cell* **177**, 1888-1902.e21
553 (2019).
554 30. Roberts, S. B. & Rosenberg, I. Nutrition and Aging: Changes in the Regulation of Energy
555 Metabolism With Aging. *Physiol. Rev.* **86**, 651–667 (2006).
556 31. Brockdorff, N. & Duthie, S. M. X chromosome inactivation and the Xist gene. *Cell. Mol.*
557 *Life Sci. CMLS* **54**, 104–112 (1998).
558 32. Lee, J. T., Davidow, L. S. & Warshawsky, D. Tsix, a gene antisense to Xist at the X-
559 inactivation centre. *Nat. Genet.* **21**, 400–404 (1999).
560 33. Liberzon, A. *et al.* The Molecular Signatures Database (MSigDB) hallmark gene set
561 collection. *Cell Syst.* **1**, 417–425 (2015).

562 34. Luo, X.-G., Ding, J.-Q. & Chen, S.-D. Microglia in the aging brain: relevance to
563 neurodegeneration. *Mol. Neurodegener.* **5**, 12 (2010).
564 35. Trapnell, C. *et al.* The dynamics and regulators of cell fate decisions are revealed by
565 pseudotemporal ordering of single cells. *Nat. Biotechnol.* **32**, 381–386 (2014).
566 36. Lemaître, J.-F. *et al.* Sex differences in adult lifespan and aging rates of mortality across wild
567 mammals. *Proc. Natl. Acad. Sci. U. S. A.* **117**, 8546–8553 (2020).
568 37. Mitchell, S. J. *et al.* Effects of Sex, Strain, and Energy Intake on Hallmarks of Aging in
569 Mice. *Cell Metab.* **23**, 1093–1112 (2016).
570 38. Kane, A. E., Sinclair, D. A., Mitchell, J. R. & Mitchell, S. J. Sex differences in the response
571 to dietary restriction in rodents. *Curr. Opin. Physiol.* **6**, 28–34 (2018).
572 39. Willard, H. F. & Carrel, L. Making sense (and antisense) of the X inactivation center. *Proc.*
573 *Natl. Acad. Sci.* **98**, 10025–10027 (2001).
574 40. Chureau, C. *et al.* Ftx is a non-coding RNA which affects Xist expression and chromatin
575 structure within the X-inactivation center region. *Hum. Mol. Genet.* **20**, 705–718 (2011).
576 41. Berletch, J. B. *et al.* Escape from X Inactivation Varies in Mouse Tissues. *PLoS Genet.* **11**,
577 (2015).
578 42. Sternson, S. M. Hypothalamic Survival Circuits: Blueprints for Purposive Behaviors. *Neuron*
579 **77**, 810–824 (2013).
580 43. Toda, C., Santoro, A., Kim, J. D. & Diano, S. POMC Neurons: From Birth to Death. *Annu.*
581 *Rev. Physiol.* **79**, 209–236 (2017).
582 44. Ma, T., Wong, S. Z. H., Lee, B., Ming, G. & Song, H. Decoding neuronal composition and
583 ontogeny of individual hypothalamic nuclei. *Neuron* (2021).

584 45. Vann, S. D. & Nelson, A. J. D. The mammillary bodies and memory. in *Progress in Brain*
585 *Research* vol. 219 163–185 (Elsevier, 2015).
586 46. Işıldak, U., Somel, M., Thornton, J. M. & Dönertaş, H. M. Temporal changes in the gene
587 expression heterogeneity during brain development and aging. *Sci. Rep.* **10**, 4080 (2020).
588 47. López-Otín, C., Blasco, M. A., Partridge, L., Serrano, M. & Kroemer, G. The Hallmarks of
589 Aging. *Cell* **153**, 1194–1217 (2013).
590 48. Leng, K. *et al.* Molecular characterization of selectively vulnerable neurons in Alzheimer's
591 disease. *Nat. Neurosci.* **24**, 276–287 (2021).
592 49. Krashes, M. J. *et al.* Rapid, reversible activation of AgRP neurons drives feeding behavior in
593 mice. *J. Clin. Invest.* **121**, 1424–1428 (2011).
594 50. Williams, K. W. *et al.* Xbp1s in Pomc Neurons Connects ER Stress with Energy Balance and
595 Glucose Homeostasis. *Cell Metab.* **20**, 471–482 (2014).
596 51. Austad, S. N. Why women live longer than men: Sex differences in longevity. *Gend. Med.* **3**,
597 79–92 (2006).
598 52. Sampathkumar, N. K. *et al.* Widespread sex dimorphism in aging and age-related diseases.
599 *Hum. Genet.* **139**, 333–356 (2020).
600 53. Costs of sexual selection in natural populations of mammals. *Proc. R. Soc. Lond. B Biol. Sci.*
601 **247**, 203–210 (1992).
602 54. Burger, J. M. S. Sex-Specific Effects of Interventions That Extend Fly Life Span. *Sci. Aging*
603 *Knowl. Environ.* **28**, 30 (2004).
604 55. Honjoh, S., Ihara, A., Kajiwara, Y., Yamamoto, T. & Nishida, E. The Sexual Dimorphism of
605 Dietary Restriction Responsiveness in Caenorhabditis elegans. *Cell Rep.* **21**, 3646–3652
606 (2017).

607 56. Davis, E. J., Lobach, I. & Dubal, D. B. Female XX sex chromosomes increase survival and
608 extend lifespan in aging mice. *Aging Cell* **18**, e12871 (2019).
609 57. Sergushichev, A. A. An algorithm for fast preranked gene set enrichment analysis using
610 cumulative statistic calculation. *bioRxiv* 060012 (2016) doi:10.1101/060012.
611 58. Wouters, J. *et al.* Robust gene expression programs underlie recurrent cell states and
612 phenotype switching in melanoma. *Nat. Cell Biol.* **22**, 986–998 (2020).
613 59. Suo, S. *et al.* Revealing the Critical Regulators of Cell Identity in the Mouse Cell Atlas. *Cell*
614 *Rep.* **25**, 1436-1445.e3 (2018).
615
616
617
618
619
620
621
622
623
624
625
626
627
628
629